nature physics

SUPPLEMENTARY INFORMATION

DOI: 10.1038/NPHYS1856

Dephasing time of GaAs electron spin qubits coupled to a nuclear bath exceeding 200 μs – Supplementary Material

Hendrik Bluhm,[1] Sandra Foletti,[1] Izhar Neder,[1] Mark Rudner,[1]
Diana Mahalu,[2] Vladimir Umansky,[2] and Amir Yacoby[1]

[1]*Department of Physics, Harvard University, Cambridge, MA 02138, USA*
[2]*Braun Center for Submicron Research, Department of Condensed Matter Physics, Weizmann Institute of Science, Rehovot 76100, Israel*

This supporting document describes the pulse hardware, design and optimization procedures, and explains details of the data analysis. It also provides further data including a measurement of T_2^*, a demonstration that coherence is not affected by dynamic nuclear polarization used to extend T_2^* (ref 1), and the field dependence of a four-pulse CPMG-echo. We discuss the background subtraction and data normalization, derive the fit model, outline the fitting procedures and compare the fit parameters to theoretical estimates.

I. INTRINSIC AND ENHANCED T_2^*

In order to measure the ensemble averaged free induction decay time, T_2^*, we introduced a difference $\Delta\tau$ between the evolution times before and after the π-pulse (see Fig. 1c) of a Hahn-echo pulse. Since for $\tau \ll T_{HE}$, the electron returns to a singlet state at $\Delta\tau = 0$, this measurement is equivalent to a standard free induction decay measurement. However, it is less susceptible to systematic errors due to finite pulse rise times. The data in Supplementary Fig. 1a exhibits the expected Gaussian decay corresponding to a Gaussian distribution of ΔB_{nuc}^z with zero mean.

Supplementary Figs. 1b,c show the Hahn-echo in the presence of a nuclear gradient that was induced and stabilized using the pulse feedback polarization scheme from ref 1. The mean gradient leads to coherent oscillations in the $\Delta\tau$ dependence (Supplementary Fig. 1b), whose dephasing time is extended relative to the intrinsic T_2^* because nuclear fluctuations are reduced. These measurements show that electron coherence is not reduced substantially by the polarization scheme. Thus, the methods of refs 1,2 to achieve universal qubit control and to reduce nuclear fluctuations via dynamic nuclear polarization do not compromise the effectiveness of dynamic decoupling. This is an important conclusion for using GaAs electron spin qubits for quantum information processing.

II. PULSE HARDWARE AND DESIGN

Because of filtering and attenuation requirements for the gate pulse signals, it is common to use different cables for the high and low frequency components and to combine them at low temperature using bias T's. These act as a low and high pass filters for the respective control lines. A resistive combiner, which would offer a frequency independent performance, is not practical because it would cause an excessively large heat load. Several previous experiments[1–4] used commercial bias T's (e.g. Anritsu K251) designed for a 50 Ω environment. These inductor based devices are prone to resonances in conjunction with the high impedance gates and DC lines. Furthermore, they have to be described, to the extent that a lumped circuit model is adequate at all, by a second order differential equation, which makes it cumbersome to compensate for their distortion of the pulses near the crossover frequency. Finally, their properties may degrade at low T and due to thermal cycling. To circumvent these problems we used a simple RC-filter consisting of a 5.1 nF capacitor (700 B series from ATC) and a 5 kΩ surface mount thin film resistor. They were installed within a few mm from the sample so that no resonances are to be expected in the relatively short impedance mismatched wiring path between the sample and the bias T. By modeling these bias T's as a perfect RC-filter with time constant $\tau_{RC} \approx 25\mu$s, we were able to apply a correction $\delta V(t) = \int_0^t dt' V(t')/\tau_{RC}$, where $V(t)$ is the desired output signal and $V(t) + \delta V(t)$ the pulse that has to be applied in order to obtain this signal. This correction is reasonably accurate for square pulses with a period of no more than about 20 μs. For pulses with a longer period, we found substantial deviations between the actual and the desired pulse shape on the gates, which most likely arise from the relatively high and frequency dependent impedance of the DC lines and their room temperature voltage dividers to ground. Our home made bias T's do not appear to degrade the pulse rise times, which are limited to approximately 2 ns by the waveform generator bandwidth (Tektronix AWG 520) and attenuation in the coaxial cables.

In many experiments, the largest fraction of a pulse cycle is spent at the measurement point. In this case, it is adequate to only apply the small corrections for the short initialization and manipulation pulses away from the measurement point according to the above model. As the manipulation times (i.e. the time the two electrons are separated) become comparable to τ_{RC} and the measurement time, the corrections become larger and thus the influence of errors in the model and its parameters grows. Furthermore, pulse dependent offsets to the low frequency control lines have to be applied because the DC part of the pulses is entirely eliminated by the bias T's.

DOI: 10.1038/NPHYS1856

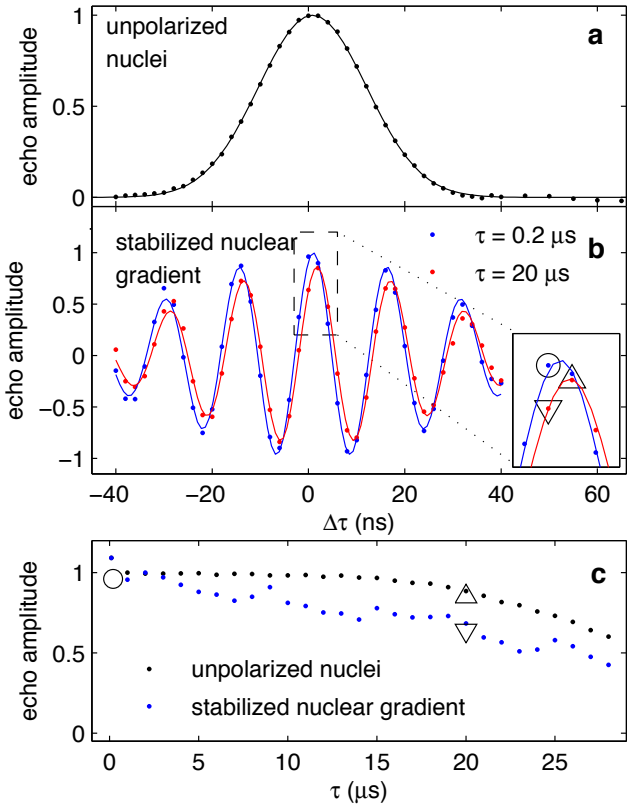

Supplementary Fig. 1: **Characterization and influence of ΔB^z_{nuc} a,** Echo amplitude for an imbalanced Hahn-echo pulse for $B_{ext} = 150$ mT and $\tau = 0.2$ μs. The fit to $\exp(-(\Delta\tau/T_2^*)^2)$ gives an inhomogeneous dephasing time of $T_2^* = 15.8$ ns. **b,** Same measurement for $B_{ext} = 0.7$ T, $\tau = 0.2$ μs and $\tau = 20$ μs in the presence of a nuclear gradient ΔB^z_{nuc} that was stabilized using the feedback dynamic nuclear polarization scheme of ref 1. From the sinusoidal fits with Gaussian envelope, we extract a T_2^* of 40 and 37 ns and a precession frequency of 65 MHz. **c,** τ dependence of the Hahn-echo under the same conditions as **b** for $\Delta\tau = 0$ and without dynamic polarization. The irregular shape and faster apparent decay of the blue trace can be attributed to shifts of the echo maximum away from $\Delta\tau = 0$, as seen in panel **b** and illustrated by the open symbols and their counterparts in the zoomed inset of panel **b**. Because of the induced nuclear gradient, this manifestation of wave function shifts is more pronounced than without polarization.

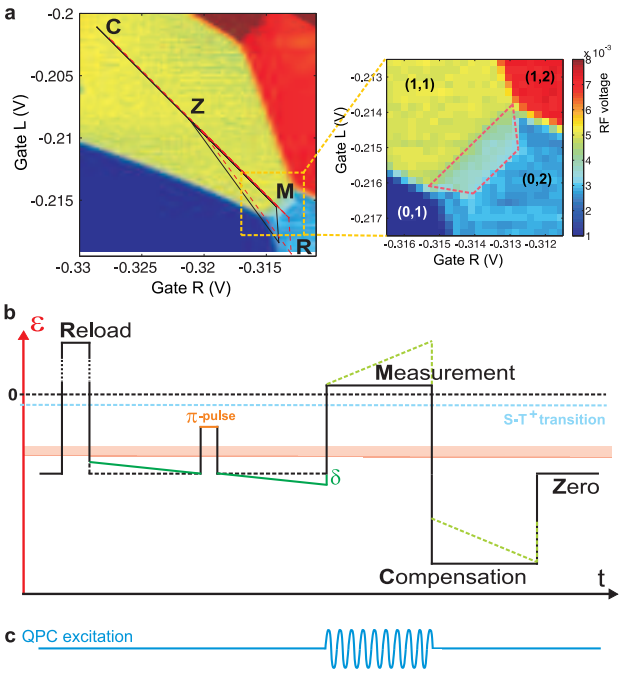

Supplementary Fig. 2: **Pulse design. a,** Scan of the QPC conductance as a function of Gates L and R. Each region corresponds to a different electron occupation number as indicated in zoomed in plot on the right. The trapezoid in that plot indicates the region where the (1, 1) triplet state is metastable and spin-to-charge conversion is possible. The contrast in this region is the result of running a pulse that generates a mixed electronic state[5]. The solid line in the left plot shows the trajectory of the spin-echo pulses in gate voltage space. The dashed line represents the same pulse, but shifted such that the measurement point is outside the readout region, thus enabling a background measurement. **b,** Schematic of the time dependence of the detuning ϵ over a single Hahn-echo pulse cycle. The letters in panel **a** indicate the positions of the pulse stages. The continuous green line with slope $2\delta/\tau$ shows the correction applied in order to compensate pulse imperfections (see Sec. III). The dashed lines show the modification of the pulse applied to compensate for the high pass filtering by the bias-T's. (We applied this correction to the whole pulse, but only show its effect for the readout stage for clarity.) **c,** The 230 MHz QPC excitation was only switched on during the measurement stage, thus avoiding backaction during the evolution stage.

For pulses with long evolution times in the manipulation stage, it is convenient to place the origin at the fully separated (1, 1) configuration and to add a pulse that is approximately the opposite of the readout pulse (which was 10 μs long in our case) after the readout stage. As a result, only very small corrections for the bias T effect are necessary during the manipulation stage, thus reducing the sensitivity to an imperfect compensation. For most measurements discussed, we used a pulse period of 50 μs, which allows evolution times τ of up to about 29 μs. For the CPMG measurements of Fig. 3, the pulse period was 250 μs. The compensation pulse and bias T corrections are illustrated in Supplementary Fig. 2b.

We monitored the conductance of our QPC charge sensor using an RF reflectometry technique[6]. Besides providing large sensitivity and bandwidth, this method allows activating the 230 MHz QPC excitation only during the readout stage of each pulse cycle (Supplementary Fig. 2c), which avoids a readout-related perturbation of the qubit in the manipulation stage. Furthermore, we record only the charge signal during the readout stage rather than averaging over the whole pulse period, thus largely eliminating undesired background signals and ex-

cess noise. The RF power level at the sample was about -91 dBm.

III. PULSE OPTIMIZATION

Even after adjusting τ_{RC} according to other characterization measurements, Hahn-echo pulses typically do not yet show the results shown in Fig. 2a for τ larger than a few μs. Relatively rapid measurements of the $\Delta\tau$ dependence (50 data points/s) show fluctuations of the position of the maximum of the echo amplitude on a time scale typical for fluctuation of the nuclear hyperfine field (Supplementary Fig. 3a). Averaging over these fluctuations leads to a reduction of the mean echo amplitude.

The observation that the maximum echo amplitude generally occurs away from $\Delta\tau = 0$ indicates that the electrons are subjected to different Overhauser fields before and after the π-pulse. We attribute this difference to a small, deterministic spatial shift of the electronic wave function arising from a drift of the gates voltages during the pulse cycle. Such a shift modifies the hyperfine coupling strength of the electron to each individual nucleus and thus changes the Overhauser fields sampled by the electron. We estimate that the dephasing time scale associated with this effect is on the order of $(\ell/\delta x)T_2^*$, where δx is the (average) displacement of the electron and $\ell \sim 20$ nm is the width of the wave function. Hence, δx has to be limited to within much less than a lattice constant to observe coherence times of tens of microseconds.

We found that this stability can be achieved by adding a compensation along the ε axis to the pulses. We have chosen a linear form for this correction (Supplementary Fig. 2b), but we expect that only the mean of the shift over each evolution interval is important. We have iteratively optimized the amplitude δ of this compensation for each mixing time by measuring the echo amplitude for three equidistant values of δ and choosing the next set of δ-values centered around the maximum of a quadratic interpolation (with a cutoff to avoid large changes in the first few steps). Once implemented, this procedure converged within no more than 10 runs, each of which required about 30 min of averaging. Supplementary Figs. 3c and d show the δ-values used for the last iteration and the resulting echo amplitudes as a function of τ, which are improved dramatically compared to the unoptimized pulses. The approximately equal reduction of the echo signal for larger or smaller δ-values confirms that we have found a local optimum. We have transferred this empirical correction to pulses with smaller τ increments used to take the data from Fig. 2a via the cubic fit shown in Supplementary Fig. 3c. Attempts to introduce additional corrections, for example orthogonal to the ε axis or by applying pulses to other gates, led to no further improvements.

To quantitatively demonstrate the plausibility of the dephasing mechanism in the absence of correction explained above, we compare to the rms hyperfine field caused by a wave function shift in response to a change in ε as estimated in ref 7 for a similar device. Using their theoretical value of an rms Rabi frequency of 11

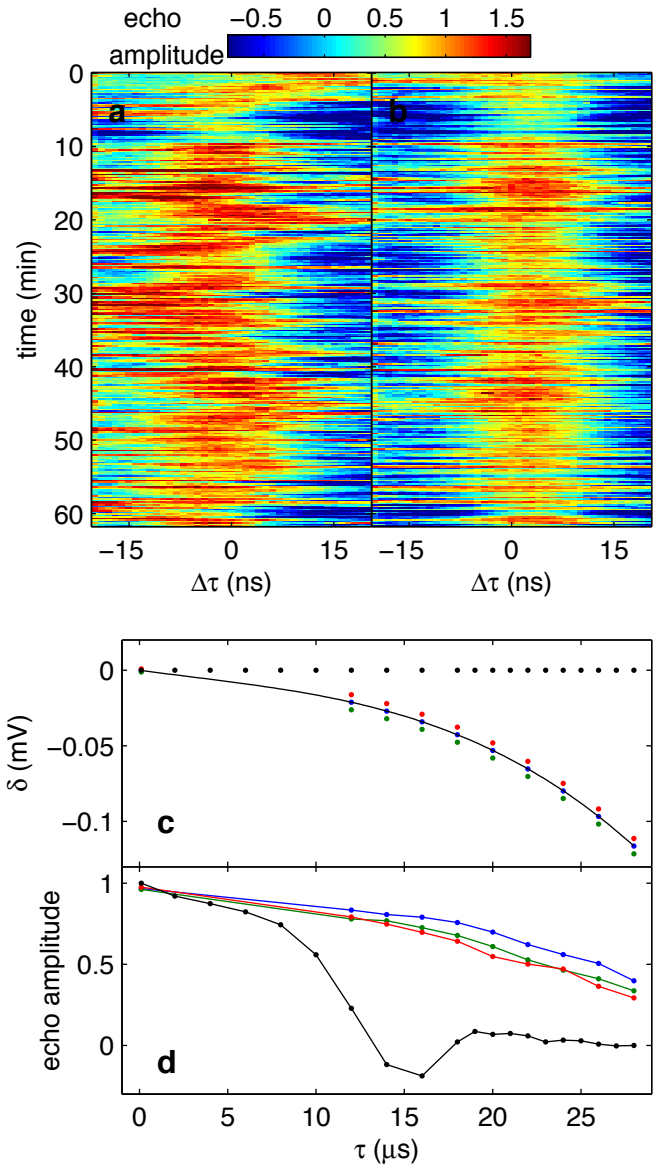

Supplementary Fig. 3: **Pulse optimization. a, b,** Repeated measurements of the echo signal as a function of $\Delta\tau$ at B_{ext} = 0.7 T, τ = 5.4 μs with unoptimized (**a**) and optimized (**b**) pulses. For unoptimized pulses, the position of the maximum of the echo signal fluctuates on a timescale typical for nuclear fluctuations. After optimization, only the width of the maximum fluctuates. Without correction, the mean echo amplitude is reduced. **c,** Correction parameter δ (see Supplementary Fig. 1b) at (blue) and near (red, green) the optimum. The black line is the cubic fit used to interpolate the correction parameter. **d,** Echo amplitude for $\Delta\tau = 0$ for the parameters in panel **c** and without any optimization ($\delta = 0$, black).

DOI: 10.1038/NPHYS1856

μs^{-1} for a modulation of 1.5 mV in ε, we find that $\delta = 20$ μV corresponds to a (Gaussian) dephasing time scale $2\sqrt{2}/11\mu s^{-1} \times 1.5\text{mV}/20\mu\text{V} = 20$ μs. Supplementary Figs. 3c,d show that the omission of a correction $\delta = 20\mu$V leads to dephasing after $\tau = 10$ μs, in reasonable agreement with the rough theoretical estimate.

We have not applied any correction to the CPMG pulses from Fig. 3. The resulting errors likely limit the coherence time observed in Figs. 3a and b, and are responsible for the bump around $\tau = 180$ μs in Fig. 3b. As we decrease the interval between π-pulses, these errors seem to be mostly eliminated, although we cannot rule out that they contribute to the linear reduction of the echo signal in Fig. 3. We expect that fewer π-pulses would be sufficient for obtaining a given coherence time if applying corrections to the gate voltages between them, however the optimization would be more complicated and time consuming due to the multidimensional parameter space.

IV. NORMALIZATION AND BACKGROUND MEASUREMENTS

Since the QPC conductance not only depends on the electron configuration of the adjacent double dot, but also on the pulsed gate voltages, an absolute measurement of the (average) electronic state generally requires some form of calibration. Here, we have taken reference measurements by omitting all π-pulses from the Hahn or CPMG sequences. The resulting pulses correspond to a T_2^* measurement which, for mixing times τ above a few 10's of nanoseconds, should produce a completely dephased state. Furthermore, we measured the response to each pulse at a point of larger positive detuning ε, where the (0, 2) triplet state has a lower energy than the (1, 1) triplet so that either spin state leads to a (0, 2) charge signal (Supplementary Fig. 2a). The latter measurements are referred to as "large detuning" or "large-ε" below. Supplementary Fig. 4a shows all four measurements for a typical Hahn-echo measurement as a function of τ. The curved overall background common to all these measurements is due to direct coupling of the imperfectly compensated gate pulses to the QPC: different pulses tend to have slightly different gate voltages in the readout phase. We estimate the time average of this unintentional variation to be on the order of 0.2 % of the gate voltage change between the free evolution point in (1, 1) and the measurement point.

The differences between the charge signal of various combinations of these pulses are shown in Supplementary Fig. 4b. When reading out at a large detuning without charge contrast, the difference between the echo and reference pulses is very small. We thus conclude that the change of the direct coupling due to the omission of the π-pulses has a negligible effect. Subtracting the QPC readout signal from identical pulses applied at different detunings should single out the contribution of the different electron charge configurations of the (0,2) singlet and (1,1) triplet states, up to a constant offset due to the different DC gate voltages. For the range of τ of Fig 2a and Supplementary Fig. 4, the mixed state shows the expected flat difference signal.

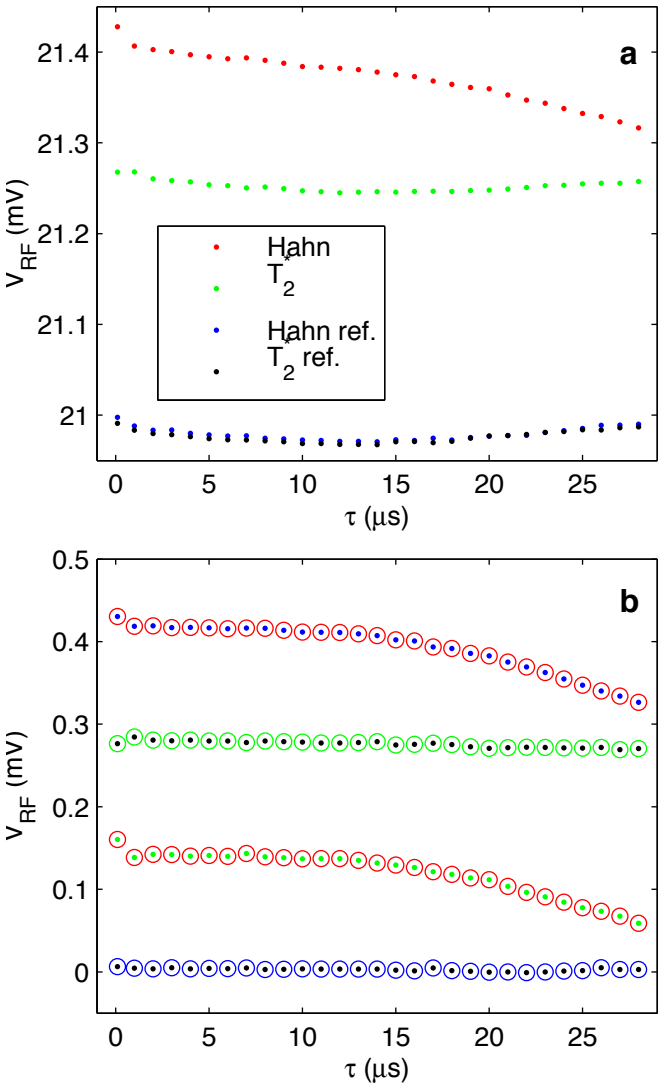

Supplementary Fig. 4: **Background subtraction. a,** Raw data for the 0.4 T Hahn-echo measurement of Fig. 2a. The T_2^* pulses are identical to the Hahn-echo pulses except for the omission of any π-pulses and produce a completely dephased state for the long τ used here. The two reference measurements were taken with the same pulses, but at a working point where both singlets and triplets lead to a (0,2) charge signal. **b,** Differences between various pairs of curves from panel **a**. The colors of the circles and dots indicate the curves that were subtracted. The red/green combination corresponds to the subtraction used in Fig. 2a for $B_{ext} \geq 0.2$ T and most other τ-dependence measurements.

Based on these findings, we employed two different background elimination schemes for the data in Fig 2a, which we will describe next. A different procedure was

used for Fig 3, as discussed further down. For most datasets in Fig. 2a, the singlet return probability and thus the echo amplitude were taken as proportional to the difference between the signals of the echo pulse and the corresponding mixed-state reference pulse. For $B_{ext} < 0.2$ T in Fig. 2a, we took no (simultaneous) reference measurement in order to measure with a higher τ resolution without exceeding the memory limitation of our waveform generator. Instead, we subtracted the signal from the echo-pulses at large detuning and used the last (few) data points as a reference to determine the constant offset. We checked the consistency of the two procedures by repeating the low-field measurements at a lower resolution, but with a reference.

In addition to the reference level, we need to determine the proportionality factor converting the measured signal difference to an echo amplitude. In principle, it could be determined from the height of the (1, 1) - (0, 2) transition, measured by sweeping the DC gate voltages. However, the actual signal is usually smaller due to inelastic decay of the metastable (1, 1) triplet state at the measurement point. The rate of this decay depends on the tuning of the gate voltages and on the nuclear hyperfine gradient, ΔB^z_{nuc}. To circumvent a complicated calibration correcting for these effects, we instead normalized the datasets in Fig. 2a by the echo amplitude obtained at short τ, but ignored the first data point. This normalization disregards the apparent signal reduction between the first two points (see Sec. VI).

On the much longer time scale of the CPMG measurements of Fig. 3, we find a linear trend in both the mixed-state reference and CPMG data after subtracting a large-ε background from either measurement. This trend appears to increase with larger B_{ext} and and also becomes visible for shorter τ above 0.4 - 0.7 T. A possible explanation is a single-spin T_1 process, which would cause leakage into the T_+ and T_- states and thus increase the triplet probability for longer τ. Such a T_1 process can be expected to be exponential and thus would be consistent with a linear initial decay. To avoid ambiguities due to this poorly understood background, we only subtracted a measurement at the large-ε working point and normalized by the DC charge transition. We refer to this quantity, which is plotted in Fig. 3, as P_S. The overall offset was chosen so that small τ give $P_S = 1$. In the absence of inelastic decay and other effects as discussed above, this procedure would lead to $P_S = p(S)$ ($= 0.5$ for the mixed state), but in practice $P_S > p(S)$.

For the $\Delta\tau$ dependence of Supplementary Figs. 1 and 5b below, we subtracted the background from the large-ε operating point, and determined the offset and scale from the fits, which amounts to setting the zero level to the signal for large $\Delta\tau$. We checked that that omitting the π-pulses gives the same result. The scale factor was again chosen so that the short-τ measurements give unity echo amplitude, and kept constant for measurements differing only by their τ value (e.g. Supplementary Figs. 1b, 5b).

Note that these normalization procedures also divide out any visibility loss due to imperfections in the preparation and π-pulse fidelity. The latter is limited by systematic errors in the pulse calibration, electrical noise, and axis errors. The π-pulse axis is not exactly perpendicular to the dephasing axis on the Bloch sphere because ΔB^z_{nuc} is not entirely negligible compared to the exchange splitting J between the S and T_0 states during the π-pulse. However, such errors should be independent of the separation time τ (apart from contributions from slow AC noise), so that they do not affect our dephasing time measurements. In order to preserve the state of the qubit regardless of its initial state, these errors will of course have to be eliminated.

We would also like to point out that our multiple π-pulse sequence is equivalent to the CPMG sequence rather than the Carr-Purcell sequence even though we do not use a $\pi/2$ pulse around the y-axis of the Bloch sphere for preparation. Instead, we rapidly switch off the exchange splitting J, which prepares an initial state on the axis around which the exchange π-pulses rotate. This state is the same as the one obtained by applying a $\pi/2$- pulse around the orthogonal y-axis after preparing a ground state $|\uparrow\downarrow\rangle$ or $|\downarrow\uparrow\rangle$, as in the original CPMG sequence.

V. CONSISTENCY CHECKS

In order to verify our interpretation of the τ-dependence measurements as a T_2 measurement and the accuracy of the π-pulses, we have measured the dependence of the echo signal on $\Delta\tau$ and the duration of the exchange pulses for various pulse sequences. The results shown in Supplementary Fig. 5 are fully consistent with expectations.

We have also retaken some of the Hahn-echo data in Fig. 2a with a longer pulse period of 80 μs, so that the complete echo decay curve can be seen even at high fields (Supplementary Fig. 6). The pulses used for these experiments were optimized as described in Sec. III. However, due to the longer period, the required correction turned out to be smaller, on the order of the last bit of our wave form generator. We believe that the discreteness introduced by this limitation is the cause for the somewhat irregular shape of the curves in Supplementary Fig. 6. Within the experimental errors and apart from the slight oscillatory structure at 0.25 T (see Fig. 2a for a detailed analysis), the data are described well by the $\exp(-(\tau/T_{HE})^4)$ over the whole τ range. However, it should be noted that the data points at the longest times may reflect a larger contribution from wave function shifts because the small echo amplitudes makes the pulse optimization less accurate. The comparison with a $\exp(-\tau^4)$ decay law rather than the more complex fit model of Eq. 3 in Sec. IX is motivated by the fact that the former is a good approximation of the latter at sufficiently high fields[8]. See Sec. VI for a discussion of the first data points.

DOI: 10.1038/NPHYS1856

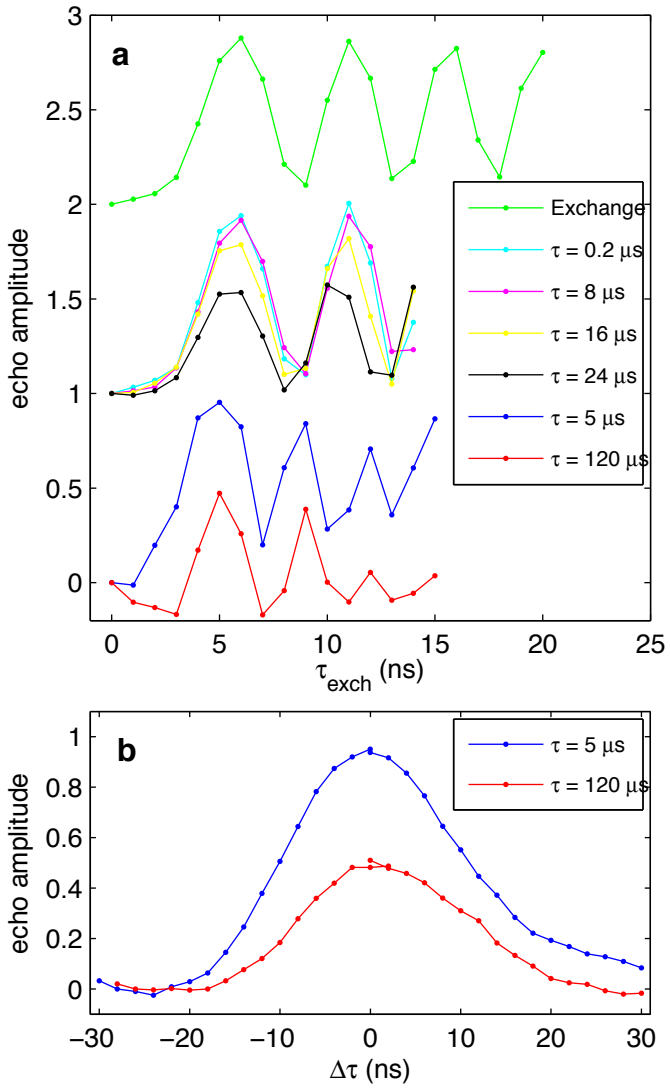

Supplementary Fig. 5: **Consistency checks. a,** Top: Exchange oscillations measured by preparing an $|\uparrow\downarrow\rangle$-state, letting it evolve at a nonzero exchange interaction for a time τ_{exch} and reading measuring the $|\uparrow\downarrow\rangle$-probability (see ref 3). Middle: Hahn-echo amplitude as a function of the duration τ_{exch} of the swap pulse. Bottom: 10 pulse CPMG-echo amplitude as a function of the duration τ_{exch} of the swap pulse. For all other measurements reported here, τ_{exch} was fixed at 5 ns. The slight frequency variations of these datasets can be attributed to pulse calibration errors and/or low frequency charge switching noise. **b,** Echo amplitude for a 10 pulse CPMG measurement as a function of a change $\Delta\tau$ of the evolution time after the last π-pulse.

VI. DEVIATION OF FIRST DATA POINT

The first data point of the τ dependence measurements typically shows a larger echo amplitude than all subsequent ones. The fact that the plotted values are larger than one is a result of the data normalization. This effect may partially reflect a measurement artifact due to

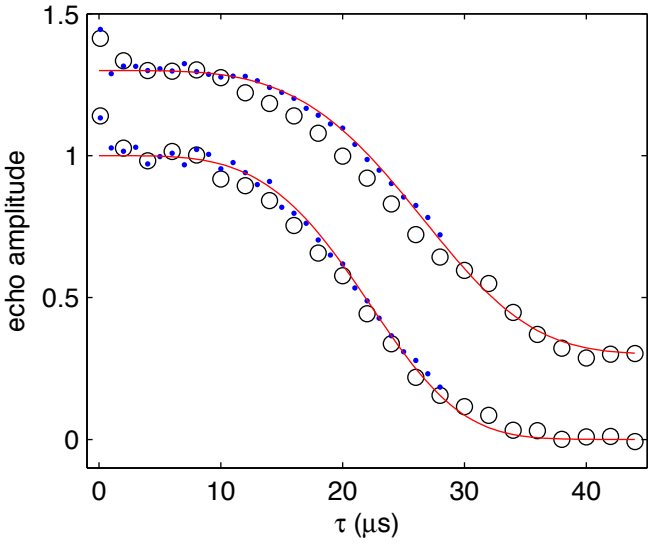

Supplementary Fig. 6: **Extended Hahn-echo measurements** at 0.25 T (bottom) and 0.4 T (top), offset for clarity. The blue dots are the same data as in Fig. 2a, taken with 50 μs period pulses. The red lines are fits of $\exp(-(\tau/T_{HE})^4)$ to these data (ignoring the first data point), with $T_{HE} = 24$ and 29 μs, respectively. The black circles were taken with pulses with a 80 μs period, and normalized by the mean of the 2, 4 and 6 μs data points. The slight deviation between the two datasets is likely due to the imperfect optimization of the 80 μs pulses which reduce the measured echo amplitude.

transients at the beginning of each measurement series, but some preliminary measurements indicated that it is a real decay of the signal on a time scale of about 0.5 μs. Such a visibility loss was predicted theoretically as a result of an initially purely electronic state being dressed by the nuclear bath[9,10], however it should be on the order of 10^{-4} rather than 0.1, as observed here. Other explanations, for example in terms of π-pulse errors, are more plausible. While potentially important and interesting, a detailed study of this effect is beyond the scope of the present work.

VII. FIELD DEPENDENCE OF CPMG-ECHO

Supplementary Fig. 7 shows the field dependence of the echo signal obtained using a four-pulse CPMG sequence, which exhibits a more complex revival structure than the Hahn-echo. Note the partial echo revival at 40 μs and 75 mT, which indicates a rather long coherence time even at relatively low fields. The decay beyond 40 μs may be an artifact of wave function shifts (see Sec. III).

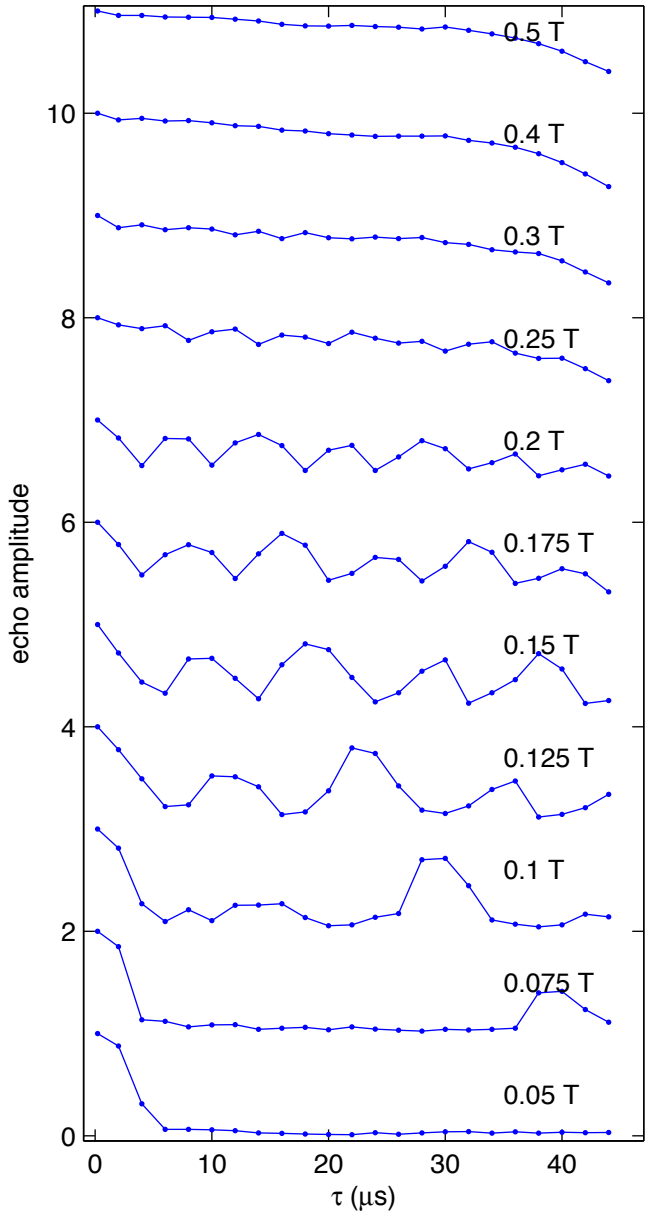

Supplementary Fig. 7: **Field dependence of the echo signal obtained using a 4 pulse CPMG sequence.** A background was measured and subtracted in the same way as for Fig. 2a (see Sec. IV), and the data normalized by the first data point. The pulses for these datasets were not optimized.

VIII. SEMI-CLASSICAL DERIVATION OF FIT MODEL

A model for decoherence of a single electron spin due to the hyperfine interaction was derived in ref 11 based on a quantum mechanical treatment of electron-mediated nuclear flip-flops. Here, we derive the same result by treating the Overhauser fields acting on the electron as semi-classical variables, which provides a simple intuition for the collapses and revivals. The heteronuclear terms in the expansion ${B_{nuc}^{\perp}}^2 = \sum_{kl}\sum_{i=x,y} A_k A_l I_k^i I_l^i$ (i.e those where nuclei k and l are of different species) oscillate at the relative Larmor frequencies $\omega_k - \omega_l$. Averaging over all initial nuclear spin states amounts to averaging over the phase and amplitude of these oscillations, which randomizes the electronic phase accumulated during an echo experiment and thus causes the collapse of the echo amplitude. However, if the free evolution time $\tau/2$ is a multiple of each of the three relative Larmor periods, the contribution of those oscillations to the electron phase vanishes regardless of the nuclear state, which leads to the revival peaks. Note that it is a fortunate coincidence that the three Larmor frequencies are nearly equidistant, so that the commensurability condition is easily fulfilled to a good approximation for all three pairs of species simultaneously.

We extend our model to allow for a spatial variation δB of the local magnetic field determining the nuclear Larmor frequencies, $B_{ext}+\delta B$. Such a variation phenomenologically accounts for the random dipolar and electron-mediated exchange field of neighboring nuclei and for possible quadrupolar shifts from the electric field associated with the electron. It leads to fluctuations of the transverse field from each nuclear species beyond a rigid rotation, which contribute to the envelope decay of the echo amplitude.

The fact that the two electrons are decoupled and interact with two independent nuclear ensembles during the free evolution allows us to begin by considering dephasing in a single dot, and then to apply the result to the relevant case of a double dot. Our notation largely follows that of ref 11. A detailed justification of our semi-classical treatment will be given elsewhere[8].

Because of their smaller g-factor, the nuclei evolve three orders of magnitude slower than the electrons. Thus, the precession of the electron spin adiabatically follows the instantaneous eigenstates aligned with the total field $\mathbf{B}_{tot} = \mathbf{B}_{ext} + \mathbf{B}_{nuc}$ and we only need to consider the level splitting $g^*\mu_B B_{tot} = g^*\mu_B\sqrt{(B_{ext}+B_{nuc}^z)^2 + {B_{nuc}^{\perp}}^2} \approx g^*\mu_B(B_{ext} + B_{nuc}^z + {B_{nuc}^{\perp}}^2/2B_{ext})$. We will thus work with the electronic Hamiltonian $\hat{H}(t) = g^*\mu_B(B_{ext} + B_{nuc}^z(t) + {B_{nuc}^{\perp}(t)}^2/2B_{ext})\hat{S}_z$. In ref 11, this effective Hamiltonian was formally derived from a Schrieffer-Wolff transformation.

In Sec. IX, we will account for fluctuations in B_{nuc}^z by assuming that they are uncorrelated with those of $B_{nuc}^{\perp}$ and lead to a field independent echo decay factor $\exp((-\tau/\tau_{SD})^4)$, as computed in ref 12. In this section, we focus on the effect of $B_{nuc}^{\perp}(t)^2$, which we write as a sum of semi-classical fields $B_{nuc}^{\perp\sigma}(t)^2 = \sum_{k,l} B_k^{\sigma}(t)B_l^{\sigma}(t)^*$. The summation indices k and l run over groups of (approximately) equivalent nuclei. Each group k includes only nuclei of the same species $\alpha(k)$, experiencing the same local field inhomogeneity δB_k, and having the same hyperfine coupling strength A_k. The $B_k^{\sigma} = B_k^{\sigma x} + iB_k^{\sigma y}$ are complex-valued with the real and imaginary part

DOI: 10.1038/NPHYS1856

representing the x and y component of the total transverse field from group k. $\sigma = \pm 1$ specifies the initial $\hat{S}^z$ eigenstate $|\sigma\rangle$ of the electron, which is important because it determines the sign of the Knight shift. For the time evolution of the nuclear field, we assume that nuclei in the group k precess at a constant Larmor frequency $\omega_k + \delta\omega_k + \sigma c(t) A_k/2$. Here $\omega_k = \gamma_{\alpha(k)} B_{ext}$ is the species $\alpha(k)$ dependent Larmor frequency, and $\delta\omega_k = \gamma_{\alpha(k)}\delta B_k$ its change due to a local field δB_k. $c(t) = \pm 1$ describes the pulse sequence and changes at every π-pulse, thus switching the sign of the Knight shift term $\sigma c(t) A_k/2$. For the Hahn-echo, $c(t) = 1$ (-1) for $t < \tau/2$ $(t > \tau/2)$. The time dependence is thus $B_k^\sigma(t) = B_k^\sigma(0) e^{i(\omega_k t + \delta\omega_k t + \frac{1}{2}\sigma A_k \int_0^t c(t)dt)}$. The relative phase Φ picked up between the two electronic states $|\sigma = \pm\rangle$ over a pulse sequence of duration τ is then given by

$$\begin{aligned}\Phi &= \frac{g^*\mu_B}{4\hbar B_{ext}} \sum_{\sigma=\pm1} \int_0^\tau c(t)dt \sum_{k,l} B_k^\sigma(t) B_l^{\sigma *}(t) \\ &= \frac{g^*\mu_B}{4\hbar B_{ext}} \sum_{k,l} \overline{B}_l \overline{B}_k z_k z_l^* \sum_{\sigma=\pm1} \\ &\quad \times \int_0^\tau c(t)dt \exp\left(i(\omega_{kl} + \delta\omega_{kl})t + i\sigma A_{kl} \int_0^t dt' c(t') \right) \\ &\equiv \sum_{k,l} T_{kl} \frac{z_k z_l^*}{2}, \end{aligned} \tag{1}$$

where we have expressed the initial conditions for $B_k^\sigma(0)$ by the dimensionless complex variables z_k and the rms transverse field values, $\overline{B}_k = \sqrt{a_{\alpha(k)} N_k n_{\alpha(k)}/2} A_k$. Furthermore, $\omega_{kl} = \omega_k - \omega_l$, $\delta\omega_{kl} = \delta\omega_k - \delta\omega_l$, $A_{kl} = (A_k - A_l)/2$, $a_{\alpha(k)} = 2/3(I_{\alpha(k)} + 1)I_{\alpha(k)} = 5/2$, and the number of nuclei of species α per unit cell, n_α, are defined as in ref 11. N_k is the number of unit cells contributing to group k. The $\{T_{kl}\}$ are identical to the coarse grained $\tilde{T}$-matrix of ref 11, except for our extension to account for the local field variation δB.

We now carry out an ensemble average over the initial conditions by treating $\{z_k\}$ as uncorrelated Gaussian-distributed random variables (justified by the large number of nuclear spins involved) with zero mean and unit variance, i.e. with probability density function $p(z, z^*)dzdz^* = \frac{i}{4\pi} \exp(-\frac{zz^*}{2}) dzdz^*$.

$$\begin{aligned}\langle e^{-i\Phi} \rangle &= \int \left(\prod_j dz_j dz_j^* p(z_j, z_j^*) \right) \exp\left(-i \sum_{k,l} T_{kl} \frac{z_k^* z_l}{2} \right) \\ &= \prod_j \int dz dz^* p(z, z^*) \exp\left(-i\lambda_j \frac{|z|^2}{2} \right) \\ &= \prod_j \frac{1}{1 + i\lambda_j}, \end{aligned} \tag{2}$$

where the $\{\lambda_j\}$ are the eigenvalues of the T-matrix, and we have used the fact that the distribution of the z_k is invariant under the basis change associated with the diagonalization of the T-matrix.

So far, we have only considered the decoherence of a single electron spin. Since the nuclei in the two halves of our double dot can be assumed to be statistically independent and the phase difference between the $|\uparrow\downarrow\rangle$ and $|\downarrow\uparrow\rangle$ states of the double dot is the sum of the single-dot phases, the two-electron decoherence function is a product of two single-dot functions: $\langle e^{i\Phi_{\text{double-dot}}} \rangle = \langle e^{i(\Phi_{\text{left}} - \Phi_{\text{right}})} \rangle = \langle e^{i\Phi_{\text{left}}} \rangle \langle e^{-i\Phi_{\text{right}}} \rangle = |\langle e^{i\Phi} \rangle|^2$, where the subscripts denote the two halves of the double dot and the last equality holds for identical dots.

IX. FIT PROCEDURES AND RESULTS

The fits in Fig. 2a were performed using the expression

$$C(\tau) = \frac{\mathcal{N}}{\prod_j |1 + i\lambda_j|^2} e^{-(t/T_{SD})^4} \tag{3}$$

derived from Eq. 2, where the $\{\lambda_j\}$ are the eigenvalues of the T-matrix given in Eq. 4 below. $\mathcal{N}$ is a scaling factor accounting for inaccuracies in the data normalization discussed in Sec. IV and the exponential envelope factor models the additional dephasing due to spectral diffusion. In general, the number of unit cells N in contact with each electron can be different for the two dots due to disorder and asymmetric gate voltages, but we found that allowing different N for the two single-dot functions does not improve the fits and thus use the same N for both dots. For the Hahn-echo, the T-matrix defined in Eq. 1 is given by

$$\begin{aligned} T_{kl} &= \frac{i g^* \mu_B \overline{B}_l \overline{B}_k (\omega_{kl} + \delta\omega_{kl})}{2\hbar B_{ext}} \\ &\quad \times 4 \frac{\cos(A_{kl}\tau/2) - \cos((\omega_{kl} + \delta\omega_{kl})\tau/2)}{(\omega_{kl} + \delta\omega_{kl})^2 - A_{kl}^2}. \end{aligned} \tag{4}$$

We found that for our fit parameters, the effect of the inhomogeneity of the hyperfine coupling arising from the spatial variation of the electronic wave function is negligible. We thus used a single hyperfine coupling constant A_k for each nuclear species, and $A_{kl} = 0$. The Gaussian distribution of the Larmor fields with standard deviation δB was approximated by five discrete values of δB_k, which were assumed to be the same for all three species. Using a finer discretization had no effect on the fit model.

Based on preliminary fits, we corrected the external field by a 5 mT offset compared to the nominal value, which can be attributed to flux trapped in our superconducting magnet. We then picked an initial set of values for the physical fit parameters below and optimized it by hand to give a good overall fit to all curves in Fig. 2a, allowing only the normalization constant $\mathcal{N}$ to vary independently at each field. Its values are $\mathcal{N} = 1.00 \pm 0.05$ except for the traces at 45, 70 and 95 mT, for which $\mathcal{N} \approx 0.90$.

The physical fit parameters are the number of nuclei per dot, N, the spectral diffusion decay time, T_{SD}, and the spread of the Larmor frequencies parametrized by δB. N determines the width of the revival peaks at low fields and the depth of the collapses at intermediate fields, whereas the other two parameters control the envelope decay. The fits to the data shown in Fig. 2a were obtained with $N = 4.4 \cdot 10^6$, $\delta B = 0.3$ mT and $T_{SD} = 37$ μs. The latter is determined mostly by the traces at 395, 495 and 695 mT. For $B_{ext} \lesssim 200$ mT, the faster envelope decay depends practically only on δB for our parameters. At $B_{ext} = 45$ mT, δB completely suppresses any revival. Note that fitting the high field data to $e^{-(t/T_{HE})^4}$ alone gives $T_{HE} = 30$ μs, which deviates from T_{SD} because δB still contributes significantly.

A quantitative comparison of T_{SD} with theory[12] is difficult because the latter depends sensitively on the shape of the electronic wave function, but a rough comparison gives good agreement. From a self-consistent Poisson-Schrödinger model, we estimate a full width at half-maximum of the transverse electronic charge density in our heterostructure of 12 nm. We thus compare with the curve for a quantum well width $z_0 = 20$ nm from Fig. 14(b) of ref 12. The fitted $T_{SD} = 37$ μs has to be multiplied by a factor $2^{1/4}$ to account for dephasing occurring for both electrons in the double dot[13]. Under these assumptions, theory and experiment match for a Fock-Darwin radius of $\ell = 25$ nm, which would correspond to $N = (32/3)\pi z_0 \ell^2 / a_0^3 = 2.3 \times 10^6$, where $a_0 = 0.565$ nm is the lattice constant of GaAs.

In pure GaAs, the measured NMR line width is about 0.1 mT. The broadening arises from a fluctuating effective magnetic field due to dipolar and indirect exchange interactions between nuclei[14,15]. The correlation time of this field is given by the time scale for dipolar nuclear flip-flops. Assuming a typical dipolar field of at most 0.1 mT, it is at least 100 μs, substantially longer than the duration of Hahn-echo experiments. Thus, the broadening can be described by the static distribution of δB_k used in our model to a good approximation. Note that the correlation time of B^z_{nuc} is even longer (up to minutes), yet the B^z_{nuc}-fluctuations are responsible for part of the electron coherence. Here, a quasistatic approximation would yield no echo decay at all.

In addition to the interactions, the nuclei will experience a static quadrupole splitting due to electric field gradients originating from the electron. We proceed to estimate the resulting second moment of the NMR line, which we identify with δB^2. We crudely model the electron as a charge density of 50 nm lateral and 10 nm vertical extent. Its direct contribution to the electric field gradient, $\frac{\partial E_z}{\partial z} \sim e/(\epsilon_r \epsilon_0 (10 \text{ nm} \cdot 50 \text{ nm}^2) \approx 7 \cdot 10^{13}$ V/m^2, is negligible. In addition, the electric field of the electron induces a field gradient at the site of the nuclei by deforming the atomic orbitals. Following Eq. 6 of ref 14, we obtain $\frac{\partial E_z}{\partial z} = R_{14} e/(\epsilon_r \epsilon_0 \cdot 50 \text{ nm}^2)$, where $R_{14} \approx 1 \cdot 10^{12}$ m^{-1} is the relevant response tensor element. The resulting rms line width broadening for the magnetic field along the [110] direction is $\sqrt{9(4I(I+1)-3)/5}/(4I(2I-1)\gamma_\alpha) Q_\alpha \frac{\partial E_z}{\partial z}$ (ref 14, Eq. 1), where Q_α is the quadrupole moment of species α. Substituting literature values, we obtain rms line widths of 0.6 to 2.5 G for the different species. The quadrupole shift is thus of the correct order of magnitude to explain the larger δB of about 3 G needed to fit our Hahn-echo data. Interestingly, the quadrupolar shift should have a pronounced dependence on the direction of the applied magnetic field. According to our model, it vanishes for B_{ext} along the [100] direction and is largest along the [111] direction. In our experiments, B_{ext} was applied in the [110] direction. Thus, a strong enhancement of the envelope decay time can be expected for B_{ext} along [100].

[1] H. Bluhm, S. Foletti, D. Mahalu, V. Umansky, and A. Yacoby (2010), (submitted to PRL), arXiv:1003.4031.
[2] S. Foletti, H. Bluhm, D. Mahalu, V. Umansky, and A. Yacoby, Nature Physics **5**, 903 (2009).
[3] J. R. Petta, A. C. Johnson, J. M. Taylor, E. A. Laird, A. Yacoby, M. D. Lukin, C. M. Marcus, M. P. Hanson, and A. C. Gossard, Science **309**, 2180 (2005).
[4] D. J. Reilly, J. M. Taylor, E. A. Laird, J. R. Petta, C. M. Marcus, M. P. Hanson, and A. C. Gossard, Phys. Rev. Lett. **101**, 236803 (2008).
[5] A. C. Johnson, J. R. Petta, J. M. Taylor, A. Yacoby, M. D. Lukin, C. M. Marcus, M. P. Hanson, and A. C. Gossard, Nature **435**, 925 (2005).
[6] D. J. Reilly, C. M. Marcus, M. P. Hanson, and A. C. Gossard, App. Phys. Lett. **91**, 162101 (2007).
[7] E. A. Laird, C. Barthel, E. I. Rashba, C. M. Marcus, M. P. Hanson, and A. C. Gossard, Phys. Rev. Lett. **99**, 246601 (2007).
[8] I. Neder, M. Rudner, H. Bluhm, and A. Yacoby, (to be published).
[9] N. Shenvi, R. de Sousa, and K. B. Whaley, Phys. Rev. B **71**, 224411 (2005).
[10] W. A. Coish and D. Loss, Phys. Rev. B **70**, 195340 (2004).
[11] L. Cywinski, W. M. Witzel, and S. Das Sarma, Phys. Rev. B **79**, 245314 (2009).
[12] W. M. Witzel and S. Das Sarma, Phys. Rev. B. **74**, 035322 (2006).
[13] W. M. Witzel and S. Das Sarma, Phys. Rev. B **77**, 165319 (2008).
[14] R. K. Hester, A. Sher, J. F. Soest, and G. Weisz, Phys. Rev. B **10**, 4262 (1974).
[15] R. K. Sundfors, Phys. Rev. **185**, 458 (1969).